

RESEARCH

Open Access



Numerical Analysis of Blast Behavior for Non-ideal Explosive ANFO in Shock-Tube Test

Hyun-Seop Shin^{1*} , Sung-Wook Kim¹, Jae-Heum Moon¹ and Gang-Kyu Park¹

Abstract

In an explosion test using a shock tube, the behavior of pressure waves can be reproduced with high reliability. However, the explosion in a shock tube occurs in a confined space. It is difficult to predict the behavior of pressure waves and its effect on various concrete specimens by using the research findings related to free-field explosions. Moreover, few studies have focused on explosive-driven shock tubes. In this study, the behavior of pressure waves in a shock tube was numerically analyzed using a finite-element analysis program. The explosive used to generate the pressure waves was an ammonium nitrate fuel oil (ANFO), which exhibits non-ideal explosion characteristics. The Jones–Wilkins–Lee (JWL) and ignition-and-growth (I&G) equations of state were used for blast-pressure calculation. The analysis results were affected by factors such as the release rate of explosive energy and the development of the pressure waves in the confined explosion. The blast behaviors, such as the low release rate of explosive energy and the resulting increase in the impulse, were analyzed using the ignition-and-growth equation. The impulse produced during the development of waves reflected by the block installed at the tube inlet exceeded that produced by the tube wall. Such behaviors that occurred at the beginning of a blast affected the process of wave propagation along the shock tube and the wave reflection due to the test specimen at the outlet of the shock tube. In this study, the blast behavior in the shock tube, which could be referenced for the analysis of blast overpressure and its effect on concrete specimens, was numerically analyzed. Further research on the structural behaviors of concrete specimens due to blast overpressure is needed.

Keywords Shock tube, Blast behavior, Non-ideal explosion, ANFO, Equation of state, JWL, I&G, Numerical analysis

1 Introduction

Blast-resistant design is frequently applied to military and industrial facilities, and recently, to civilian infrastructures to prevent and counter the increasing terrorist threat. Blast-resistant performance of those protective facilities is usually verified by experimental

and numerical methods. Experimental methods typically include free-field tests and tests using blast simulator facilities such as a shock tube. For free-field tests, testing is conducted in a test arena with multiple targets at different distances around a single charge. While it is possible to conduct multiple tests at once, weather conditions may affect test results, and the use of large charges is limited due to noise, vibration and safety restrictions (Gan et al., 2020).

In comparison, the shock tube is an experimental facility that can reliably reproduce the behaviors of shock-waves propagating at high speeds and pressures due to the blast of explosive materials. It has the advantage of allowing the experimenter to apply the desired blast

Journal information: ISSN 1976-0485 / eISSN 2234-1315.

*Correspondence:

Hyun-Seop Shin
hsshin@kict.re.kr

¹ Department of Structural Engineering Research, Korea Institute of Civil Engineering and Building Technology (KICT), Goyangdaero 283, Ilsanseo-Gu, Goyang-Si, Gyeonggi-Do 10223, Republic of Korea

pressure to the target object reliably and repeatedly by adjusting the amount of explosive and the installation location within the capacity of the equipment (Balan & Raj, 2023; Gan et al., 2020; Stolz et al., 2016). Shock tubes are largely classified as gas-driven or explosive-driven. In this study, blast behaviors in an explosive-driven shock tube were analyzed using FEA method. Balan and Raj's review article (2023) provides an overview of the wide applications for shock tubes. Their review focuses on shock tube testing for applications like shock and blast resistance of composite materials, the behavior of joints and bolts under shock loads, manufacturing processes using shock waves, and so on. Gan et al.'s study (2020) aimed to demonstrate the ability of a newly designed shock tube in accurately generating a far-field blast environment. Stolz et al. (2016) explained how shock tube tests are used for the derivation of dynamic resistance parameters of building components. These parameters were used in single-degree-of-freedom (SDOF) models.

Many studies have focused on blasts in the free-field condition, including UFC 3-340-02 (Dobrocinski & Flis, 2015; Friedlander, 1946; Karlos et al., 2016; Kingery & Bulmash, 1984; Lim et al., 2016; Rigby et al., 2020; USACE, 2008; Yang et al., 2021). However, in the case of a blast within a shock tube, which is a confined explosion, the behavior of the fluid material resulting from the blast differs significantly from that for a blast in the free-field condition (Changyou et al., 2017; Hu et al., 2011; Park et al., 2021; Salvado et al., 2017). When an explosion occurs in a confined structure, not only the peak overpressure is higher than that of free air explosion, but also the duration of the blast wave is longer. This also causes the impulse, defined as the area of the pressure–time curve, to increase (Hu et al., 2011). If a free air explosion is simulated using a shock tube, much less explosive charge mass is required. For example, according to Kevin et al. (2013), 'a scenario with 1000 kg TNT-equivalent at a distance of 80 m can be reproduced with 425 g TNT in a shock tube with a diameter of 2 m.' The results of studies such as UFC 3-340-02, which is referenced often in relation to blasts in the free-field condition, are difficult to apply directly to the prediction of blast behavior in a shock tube. Therefore, it is also difficult to assess the effect of pressure waves on protective walls and many other concrete specimens. This is because the blast behavior in a confined explosion depends on the geometric shape of the structure surrounding the explosive, and on reflection of waves by the surrounding structures. The next factor that must be considered is the type of explosives used in the test, along with the appropriate analysis method for these explosives. For example, explosives such as trinitrotoluene (TNT) have the characteristic of ideal explosion that releases a large amount of energy in

a single moment. In contrast, widely used commercial explosives such as ammonium nitrate fuel oil (ANFO) are characterized by non-ideal explosion, such as relatively long chemical reactions and energy release (Johansson, 2011; Kittel et al., 2016). Finite-element analysis (FEA) has been conducted to analyze blast behaviors, and the equation of state (EOS) is used to calculate the blast pressure. One example is the Jones–Wilkins–Lee (JWL) equation (Lee et al., 1968), which is often used in ideal explosion cases. In some studies (Dimitraki et al., 2021; Figuli et al., 2020; Grisaro et al., 2021; Mahmood et al., 2020; Trofimov & Shipovskii, 2020), the JWL equation was used for non-ideal explosions. Nonetheless, researchers (Johansson, 2011; Kittel et al., 2016; Miao et al., 2022; Yi et al., 2020) have claimed that the JWL equation is more suitable for ideal explosions because it does not consider the reaction rate of the explosives. The JWL equation of state, which is based on the Chapman–Jouguet (CJ) theory and assumes that explosion occurs instantaneously in a narrow reaction zone, is considered to be inaccurate for simulating non-ideal explosion (Miao et al., 2022). According to Stimac et al.'s study (2021), detonation velocity and blast pressure of explosives with the non-ideal explosion characteristics, calculated theoretically applying the CJ theory, are significantly higher than experimentally measured.

Blast wave behaviors in the free-field have been studied experimentally and numerically by many researchers. For well-known explosives such as TNT (trinitrotoluene), if the explosive charge mass and stand-off distance are given as initial conditions, the blast pressure, positive phase duration, impulse, etc., can be predicted without much effort. However, for safety and security restrictions, studies related to explosive-driven shock-tube tests are very limited and rarely published. Furthermore, it is difficult to predict blast wave behaviors in a confined explosion from the research finding on a free-field explosion. Thus, numerical analysis is necessary to predict the blast behavior in the shock tube and make a proper test plan. JWL EOS is one of the most well-known equations of state used to calculate blast pressure, but it has limitations in simulating non-ideal explosion. Nevertheless, because the JWL EOS is represented in the form of a single simple equation, it is often used to calculate the blast pressure without considering the explosion characteristics of explosives. However, with regard to the shock-tube test, it is unknown how accurately the blast wave behavior in the confined condition can be analyzed. Thus, it is necessary to clarify the differences in blast wave behaviors depending on the analysis methods by comparing the results obtained using the equation of state suitable for

a non-ideal explosion with the results obtained using the JWL EOS.

In this study, FEA method was used to investigate the blast behaviors when explosives with non-ideal explosion characteristics are used in a shock-tube explosion test. A shock-tube model was generated by referring to an explosion test (KICT, 2022; Park et al., 2023) using the ANFO explosive, and it was analyzed using the Arbitrary Lagrangian–Eulerian (ALE) numerical simulation technique of LS-DYNA (LSTC, 2020), which is a universal finite-element program widely used for explosion analysis. The blast pressure obtained from the FEA was compared with the test result, and the development and propagation of the pressure wave due to the blast were analyzed. The JWL EOS and the ignition-and-growth (I&G) EOS, which includes the concept of the reaction rate, were used for simulations of the same conditions. Then, the differences in the blast behavior in the shock tube were examined. Thus, it was possible to analyze the blast behaviors in an explosive-driven shock tube, such as the development and propagation of pressure waves, which are difficult to analyze via explosion tests. Furthermore, the factors affecting the behaviors of pressure waves were confirmed when explosives with non-ideal explosion characteristics, such as ANFO in the case of this study, are used in shock-tube explosion tests. In this study, the blast behavior in the shock tube test with non-ideal explosives was numerically analyzed. This fundamental study related to blast-loads assessment could be used as a reference for further research of the effect of blast overpressure on the behaviors of blast-resistant walls and many other concrete protective structures.

2 Equations of State for Blast-Pressure Calculation

When an explosive is ignited and undergoes the explosion process, it can be divided into three main zones according to its degree of reaction: the detonation product zone, where there are byproducts from the completed chemical reaction; the unreactive explosive zone; and the reaction zone, where the chemical reaction occurs intensively. For high explosives such as TNT, the reaction zone is short and can be neglected. It is characterized by the “ideal explosion”, where the release of energy from the explosion occurs instantaneously (Johansson, 2011). The JWL EOS, which was briefly introduced in the previous section, is based on this phenomenon and expresses the relationships among the changes in volume and energy and the pressure in a chemical reaction. It is expressed as follows (Lee et al., 1968):

$$P = A \left(1 - \frac{\omega}{R_1 V} \right) e^{-R_1 V} + B \left(1 - \frac{\omega}{R_2 V} \right) e^{-R_2 V} + \omega \frac{E}{V}, \tag{1}$$

where P represents the pressure generated by the chemical reaction of the explosive; V represents the relative volume; and $A, B, R_1, R_2,$ and ω are the material constants of the explosive.

In contrast, a chemical reaction that occurs over a long period of time in a relatively long reaction zone is called a non-ideal explosion. ANFO explosives, which are the subject of this study, belong to this category. The reaction zone was ignored in the development of the EOS for ideal explosions, but it must be considered for non-ideal explosions. For example, the I&G model defines the pressure generated in the reacted and unreacted explosive zones as separate equations (I&G EOS), as given by Eq. (2) and (3), respectively. The rate of the transition from the unreacted explosive zone to the reacted explosive zone is governed by the “reaction rate equation”, i.e., Eq. (4) (Johansson, 2011; Kittel et al., 2016; Yi et al., 2020). In the equations below, $P, V,$ and T represent the pressure, relative volume, and temperature, respectively; $r_1, r_2, r_3, r_5, r_6, a_p, b_p, xp_1, xp_2,$ and g_p are material constants; and λ is a variable that determines the volume occupied by each of the two sections, which is called the “volume fraction”. Furthermore, ρ_0 and ρ represent the initial and current densities, respectively, and $I, a, b, c, d, x,$ and y are material constants:

$$P_e = r_1 e^{-r_5 V_e} + r_2 e^{-r_6 V_e} + r_3 \frac{T_e}{V_e}, \tag{2}$$

$$P_p = a_p e^{-xp_1 V_p} + b_p e^{-xp_2 V_p} + g_p \frac{T_p}{V_p}, \tag{3}$$

$$\frac{d\lambda}{dt} = I (1 - \lambda)^b \left(\frac{\rho}{\rho_0} - 1 - a \right)^x + G (1 - \lambda)^c \lambda^d P^y \tag{4}$$

ANFO is one of the representative explosives that exhibit non-ideal explosion characteristics. According to experimental and numerical studies (Bohanek et al., 2022, 2023; Esen, 2008; Fabin & Jarosz, 2021; Jackson, 2017; Kittel et al., 2016) on ANFO explosion under confinement, its explosion properties such as the detonation velocity and blast pressure are significantly affected by charge diameter and confinement. According to the Fabin & Jarosz’s study (2021), “the detonation velocity might go as low as 40% of the ideal detonation velocity.” Thus, it is accepted by many researchers that there are limitations in simulating non-ideal explosion using the JWL EOS, which cannot take into account the energy release rate of the explosive and changes in the detonation velocity depending on charge diameter and confinement. Bohanek et al. (2023) studied experimentally and numerically the shock initiation of ANFO and the effects

of charge diameter, booster mass, and confinement on initiation behavior. It was demonstrated that the I&G EOS is capable of correctly simulating experimentally observed shock initiation of ANFO, as well as the effects of charge diameter, booster mass, and confinement. Referring to the above research results on ANFO explosive, I&G EOS was also used in this study to simulate the explosive-driven shock-tube test.

3 Description of Finite-Element Model

3.1 Initial Condition

An explosion test using a large-scale shock tube with a diameter of 1 m and a length of 15 m was conducted with the cooperation of the Agency for Defense Development (ADD) (KICT, 2022; Park et al., 2023). The explosive used in the test was ANFO, which has non-ideal explosion properties. The explosive charge masses used were 1, 2, and 3 kg, and seven tests were conducted for each explosive charge mass. The explosive was placed in a paper container. The diameter of the explosive installed in a cylinder shape remained constant and only the length increased as the explosive charge mass increased. Therefore, the confinement effect of the container and size effect were presumed to be negligible (Esen et al., 2005; Jackson, 2017; Johansson, 2011).

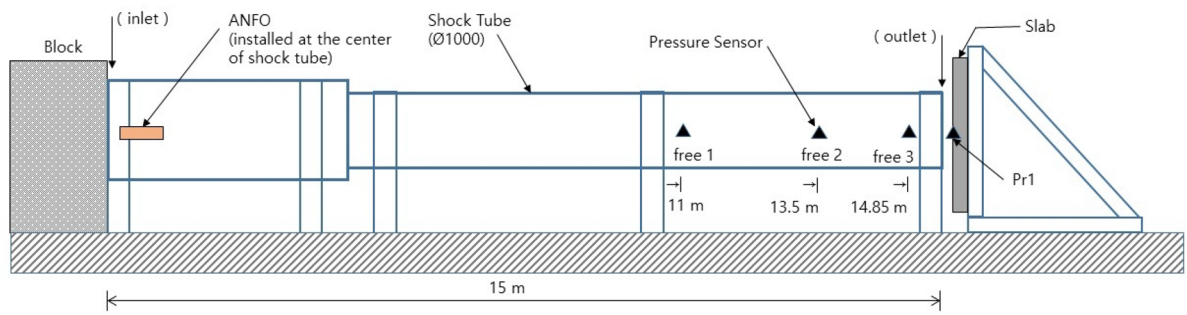
Referring to a technical data sheet provided by the explosive manufacturer H○○○, maximum density of the explosive used was 0.82 g/cm^3 , and ratio of AN (ammonium nitrate) and FO (fuel oil) is known to be close to 94:6. Furthermore, ANFO is not detonator sensitive, thus it must be initiated by a booster. Booster used in the shock-tube tests was Mega○○○ ($\rho \approx 1.20 \text{ g/cm}^3$) weighing 100 g, a type of emulsion explosive, and was produced by the same manufacturer. Although a much smaller amount of booster was used compared to the main explosive, it cannot be concluded that it had no effect on blast wave behaviors. However, within the scope of this study, since the booster amount was a constant and not a variable, it did not affect the conclusions obtained from the experiment and FE analysis. As a reference for further study, according to Bohanek, et al.'s study (2023), as the amount of booster increases, minimum detonation velocity increases and detonation velocity reaches the steady state more quickly, but the velocity in the steady state is not significantly affected by the amount of booster. Unless booster amount used differs by several tens of times, the detonation velocity does not seem to show significant variation in practice. Under the assumption that the amount of booster is significantly smaller than that of the main explosive, the effect of the booster is expected to be limited to a very local scope. This needs to be reviewed through further studies.

Fig. 1 shows the test setup. A concrete block was installed at the inlet of the shock tube near the explosive, and a concrete slab with dimensions of $1800 \text{ mm} \times 1800 \text{ mm}$ was placed in front of the outlet of the shock tube. There is a certain gap between the concrete slab specimen and the shock tube outlet. This is because the purpose of using shock-tube equipment is not to simulate a confined explosion, but to simulate a free-field explosion. Because the block used in the experiment was heavy, no movement was observed with $< 3 \text{ kg}$ of the ANFO explosive. The slab placed in front of the shock-tube outlet was fixed by a steel frame and directly received the pressure from the shock-tube outlet generated by the explosion. Three pressure sensors were installed inside the shock tube (free 1, free 2, and free 3), and one was installed at the center of the concrete slab (Pr1). The pressure sensors inside the shock tube measured the incident pressure, and the one on the slab measured the reflected pressure.

3.2 Finite-Element Model

The shockwave from the explosion causes a rapid pressure change in the air surrounding the explosive. The ALE (Arbitrary Lagrangian–Eulerian) method was used to analyze the interaction of the fluid with the structure in the flow field (Carriere et al., 2009; LSTC, 2020; Rebelo & Cismasiu, 2017; Rigby & Sielicki, 2014; Zakrisson et al., 2011). It can model the explosive, air, shock tube, and structures at the inlet and outlet of the shock tube. The fluid–structure interaction can be considered by applying constraints between the two domains. The ANFO explosive and air are modeled using the Eulerian method, whereas the shock tube and structures at the inlet and outlet of the shock tube are modeled using the Lagrangian method.

The finite-element program LS-DYNA was used for analysis, and the JWL and I&G EOSs were used to calculate the pressure generated by the ANFO explosive. The relevant constant values were entered using input cards such as JWL and IGNITION_AND_GROWTH_OF_REACTION_IN_HE. Furthermore, when the JWL EOS was used, the input card HIGH_EXPLOSIVE_BURN was used as the material model for the explosive (density, $\rho = 0.83 \text{ g/cm}^3$; detonation velocity, $D = 3879 \text{ m/s}$; CJ pressure, $P_{cj} = 3253 \text{ MPa}$). In addition, when the I&G EOS was used, the explosive density was entered using the NULL input card. An emulsion booster ($\rho = 1.20 \text{ g/cm}^3$, $D = 5500 \text{ m/s}$) was used for the detonation, and was considered in the model. For air, LINEAR_POLYNOMIAL ($C_0 = C_1 = C_2 = C_3 = C_6 = 0$, $C_4 = C_5 = 0.4$) was used as the EOS, and NULL ($\rho = 1.225\text{E-}3 \text{ g/cm}^3$) was used as the material model.



(a) Test setup



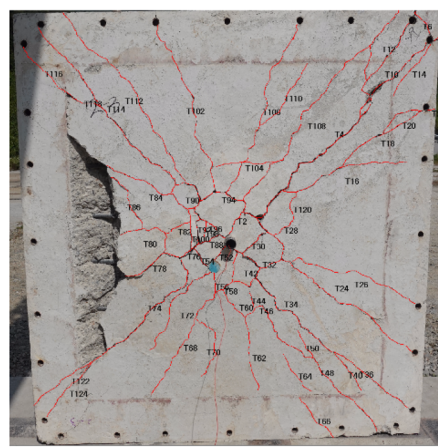
(b) Shock-tube facility



(c) Installation of the explosive



(d) Installation of specimen



(e) Test result

Fig. 1 Shock-tube test (KICT, 2022)

In the FE model, the explosives and air were modeled using solid elements, each of which has eight nodes. When fluid or fluid-like materials, such as the explosives and air in the case of this study, are modeled using the ALE method in the FE program, the multi-material ALE formulation (ELFORM=11 in SECTION_SOLID

keyword) should be applied, which makes it possible for each element to contain a mixture of different materials. Furthermore, cylindrical shape of the explosive can be modeled using automatic mesh generation algorithms as well as INITIAL_VOLUME_FRACTION_GEOMETRY input card in LS-DYNA. Commands

linked to the keywords in the input card automate the assignment of initial volume fractions to ALE elements of the explosive and the air surrounding it.

The shock tube, concrete block, and slab were modeled as rigid or elastic bodies. Because the failure behavior of the slab under blast pressure was beyond the scope of the study, the slab was modeled as an elastic body with the same stiffness as the concrete. This is similar to the computational fluid dynamics (CFD) analysis of fluid flow phenomena and pressure changes under the assumption that the structure is a rigid body. Furthermore, the shock tube used in the test was assumed to be a rigid body, as it was designed to have almost no deformation for an explosive (ANFO) charge mass of approximately 3 kg. Similarly, the concrete block installed at the inlet of the shock tube was assumed to be a rigid body. This modeling and analysis method not only reduces the numerical errors caused by the nonlinear behavior of the structure but also significantly reduces the runtime required for ALE analysis. In the FE model, the shock tube was modeled using shell elements, and the concrete block

and slab was modeled using solid elements. The material model used for the shock tube and concrete block was MAT_RIGID input card in LS-DYNA, and the slab is modeled by material model, MAT_ELASTIC. If investigation of the failure behavior of concrete material had been included in the scope of the study, the slab and concrete block would have been modeled using a nonlinear model such as Karagozian & Case concrete model (CONCRETE_DAMAGE_REL3 input card in LS-DYNA).

The constant values related to the material model among those used in the analysis were mentioned above. The constant values for the EOSs are presented in Table 1. The constants used in the analysis were selected with consideration of the density and detonation velocity provided by the explosive manufacturer. A two-step reaction process of ignition and growth was taken into account in the I&G EOS, including the selection of constants. As a boundary condition, all the displacements of the shock tube were fixed. The concrete block was allowed to move in the acting direction of the pressure wave, but other displacements were fixed. In the case of the slab, the displacements along the outer boundary were fixed. The resulting finite-element model is shown in Fig. 2.

For a mesh sensitivity analysis, the mesh size of the air was adjusted to 50, 20, 10, and 5 mm, and the FEA was performed under the same conditions. The mesh size of the structure was kept approximately the same as that of the air. When the maximum pressure (the maximum reflected pressure on the slab) from the model with a 5-mm mesh was set to 100, pressures of 98.9 (10 mm), 95.7 (20 mm), and 78.5 (50 mm) were obtained. The model with a 20-mm mesh exhibited an error within 5%. Considering the long runtime of >720 h for the model with a 5-mm mesh, a model with a 10-mm mesh was used for the FE simulation of this study. Using a mesh

Table 1 Constants of the JWL and I&G EOSs (Jayasinghe et al., 2017; Sanchidrian et al., 2015; Stimac et al., 2021)

JWL	A (MPa)	B (MPa)	R_1	R_2	ω
	2.318E5	3.414E3	6.76	1.07	0.36
I&G	r_1 (MPa)	r_2 (MPa)	r_3 (MPa/K)	r_5	r_6
	1.5E5	-2.0E3	0	11.0	15.0
	a_p (MPa)	b_p (MPa)	x_{p1}	x_{p2}	g_p (MPa/K)
	1.518E5	7.15E2	5.0	1.0	0.29
	I (1/ms)	G ($10^{-11} \mu s^{-1} Pa^{-\gamma}$)	a	b	c
	1.0E4	25	0.2	0.22	0.22
	d	x	y	-	-
	0.67	4.0	0.9	-	-

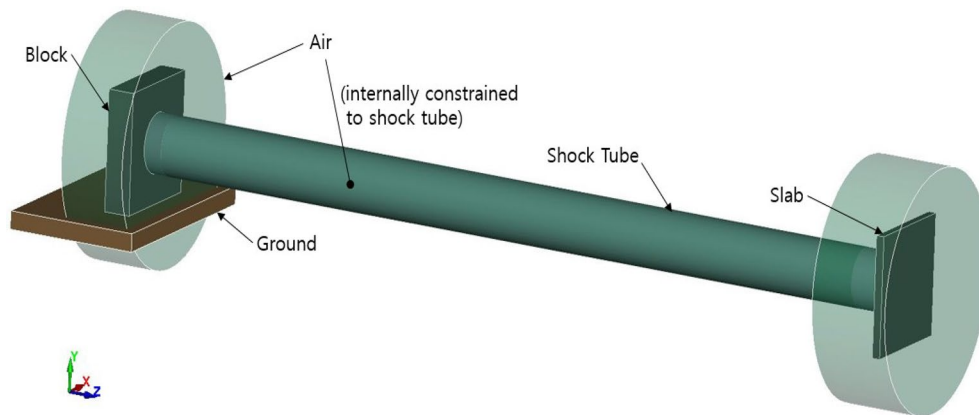


Fig. 2 Finite-element model

size of ≤ 5 mm may cause a larger pressure change. However, this change is expected to be insignificant, according to the sensitivity analysis. Furthermore, a mesh size of 10 mm was determined to be the most appropriate because the objective of this study was to analyze the blast behavior by comparing the results obtained using the JWL and I&G EOSs. Fig. 2 shows an FE model for which a total of 5,475,840 elements were used, including 97,280 SHELL elements for the shock tube and 5,378,560 SOLID elements for the explosives/air/block/slab. The mesh consisted of 5,594,892 nodes in total.

The analysis procedure in this study is shown in Fig. 3. The FE model described above was generated as given in the initial condition. The main procedure in the analysis consists of three steps: (1) visual comparison of pressure distribution generated during an early stage after ignition, and pressure distribution generated in the process of pressure-wave propagation in the shock tube, (2) comparison of incident and reflected pressure obtained using the JWL and I&G EOSs, and verification of the FE model by comparing the analysis results with test results, (3) confirmation of the factors affecting the behaviors of pressure waves in the shock tube. And finally, the influence of the factors on blast behaviors in the shock tube was quantitatively examined through a comparison of impulse graphs.

4 Results

4.1 Explosion and Shockwave Propagation

Through the FEA, the process of pressure-wave propagation in the shock tube was analyzed by observing the changes in the pressure distribution over time (Atoui

et al., 2022; Kim et al., 2022). The results obtained using the I&G and JWL EOSs were compared, where a G value of $15 (10^{-11} \mu s^{-1} Pa^{-0.9})$ was assumed for the analysis using I&G EOS as a constant in the reaction rate equation given by Eq. (4). Additionally, the explosive charge mass used in the comparative analysis was 3 kg. When the explosive was ignited, a high pressure was instantaneously generated and propagated into the surrounding air. The pressure distribution in the vicinity of the explosive at the beginning of the explosion is presented in Fig. 4a and f. As shown, the pressure was more widely distributed on the sides and below the explosives rather than on the top. This is because the ignition point was at the bottom of the explosives. At the same point in time, the JWL model exhibited an overall circular distribution of pressure, whereas the I&G model exhibited a distribution that was more biased toward the bottom of the charge.

The pressure wave that propagated in the air was reflected by the wall of the shock tube and the concrete block obstructing the inlet and was amplified, as shown in Fig. 4b and g. As shown, the two pressure distributions were compared with regard to the time when the waves reflected by the shock-tube wall began to overlap (A and A'). When the distribution shapes of the pressure reflected by the walls on the left and right sides of the explosive were compared, the I&G model exhibited a convex shape at the center (A), whereas the JWL model exhibited a more convex shape at the upper side (A'). Moreover, the pressure propagated directly from the explosive, and the pressure waves reflected by the wall overlapped on the con'c block. In the case of the I&G model, the higher pressure reflected by the block was

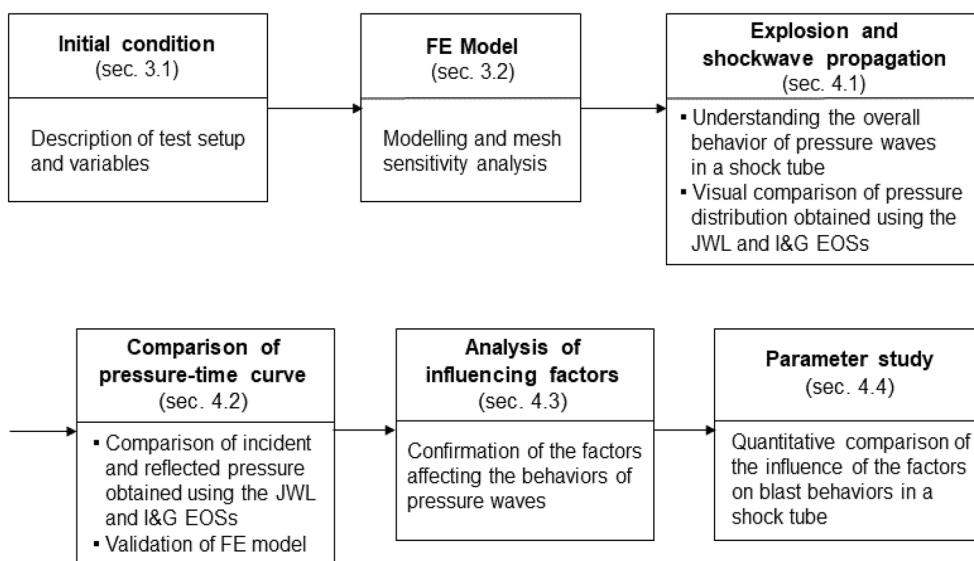


Fig. 3 Flowchart of analytical procedure

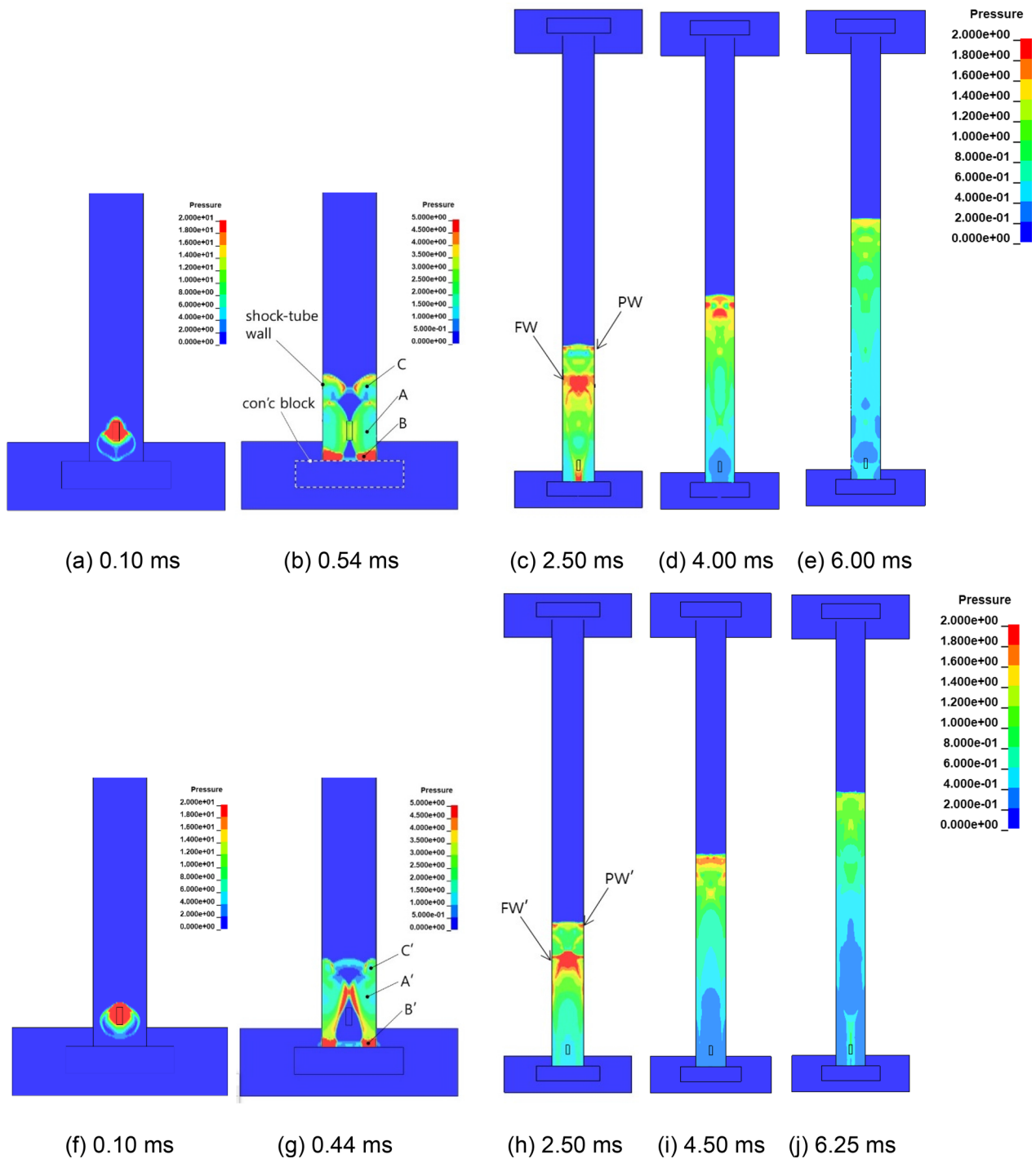


Fig. 4 Pressure contours in the shock tube **a–e** for the I&G model and **f–j** for the JWL model: **a, f** early stage after ignition; **b, g** stage in which waves reflected by the tube wall overlap; **c, h** stage in which the following wave front is formed; **d, i** stage where the preceding and following wave fronts overlap; **e, j** stage in which they propagate as a single pressure wave front

distributed over a wider range (B). Some of the pressure that propagated to the top of the explosive reached the shock-tube wall, generating another reflected wave (C and C').

After overlapping and development with the reflected waves from surrounding wall sections, the reflected waves began to propagate in the axial direction of the shock tube, similar to a merged wave. It was a preceding

wave in the sense that it was the first pressure wave that propagated to the outlet of the shock tube (PW and PW'). As a case of using the I&G model, two pressure wave fronts with a certain interval are shown as in Fig. 4c. The "preceding wave front (PW)" was generated by the shock-tube wall as the starting point. The wave reflected by the concrete block gradually developed and took the form of another wave front following the preceding wave front, which was called the "following wave front (FW)". The pressure at the preceding wave front was 1.3 MPa, and the pressure at the following wave front was 3.8 MPa; i.e., the pressure at the following wave front was nearly three times higher. In contrast, the difference in the pressures between the preceding and following waves, i.e., 1.4 and 2.3 MPa, respectively, was relatively small in the analysis using the JWL model.

As shown in Fig. 4d, the following wave front propagated at a slightly higher velocity, and it began to overlap

with the preceding wave front at approximately 4.0 ms. After this point, the pressure difference between the preceding and following waves decreased. As shown in Fig. 4e, they propagated as one wave from approximately 6.0 ms. Both the time at which the preceding and following waves began to overlap and the time at which they propagated as one wave were slightly earlier in the I&G case.

4.2 Comparison of Pressure–Time Curves

Fig. 5 presents a comparison of the pressure–time curves obtained using the FEA with the test results. The reflected pressure calculated at the center of the slab in front of the outlet of the shock tube was compared with the test data. In addition, the test data measured by the incident pressure sensor (free 1, see Fig. 1) installed in the shock tube were compared with the analysis results, for example, when 3 kg of ANFO was used. In the explosion

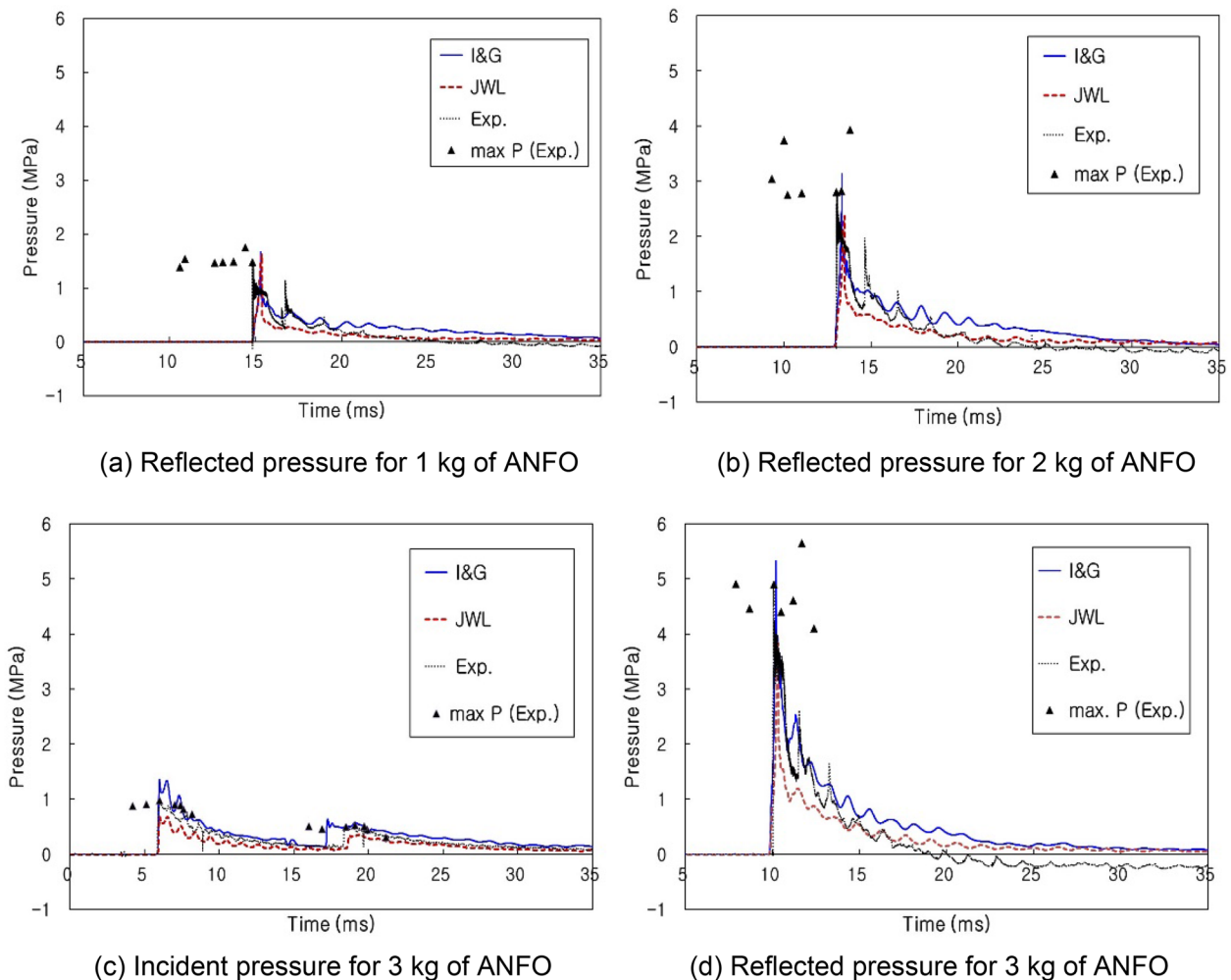


Fig. 5 Incident and reflected pressure–time curves

test referenced in this study, seven tests were conducted for each of the explosive charge masses of 1, 2, and 3 kg (KICT, 2022; Park et al., 2023). Fig. 5 shows an example of the test results. The entire pressure–time history is presented for one case in comparison with the analytical results, and the maximum values of the reflected or incident pressure are shown for the other cases. In the case of the incident pressure, two different peaks occurred. Thus, the experimental maxima were shown separately. Furthermore, the arrival times of the pressure waves obtained via the simulation differed from those measured in the experiment by up to 1–2 ms. Fig. 5 shows the graph after adjustment to the same arrival time for comparison. Tables 2 and 3 present the total measured reflected and incident pressures (free 1, see Fig. 1) for the detonation of 1–3 kg of ANFO, along with the simulation results. In addition, the impulse results are compared. Because the impulse is equal to the area under the pressure–time curve, it can be used to indirectly compare the distributions of the curves.

For example, the results obtained using the I&G model for a 3-kg ANFO explosion indicated that the peak pressure was 4.79 MPa for the experimental mean (the mean excluding the maximum and minimum) and 5.33 MPa

in the simulation. Thus, the analysis result was approximately 11% larger than the experimental result. This difference could be due to the size of the mesh used in the FE model or the assumed material constants. However, another major contributing factor is the assumption of the concrete slab as an elastic body that does not crack and fail.

When the results obtained using the JWL model for the same explosive charge mass were compared, the peak pressure was relatively low (at 3.83 MPa), and the entire curve was lower than the experimental results and the I&G case. This difference in the overall distribution patterns of the curves also appeared in the results for other explosive charge mass, as shown in Fig. 5a and b. Furthermore, Fig. 5c presents a comparison of the measured incident pressure in the shock tube with the FE results for an explosive charge mass of 3 kg. A comparison of the experimental and FE results for 1- and 2-kg explosive charge masses is presented in Table 3. Similar to the reflected-pressure comparison, the time–history curve obtained using the JWL model was lower than that obtained using the I&G model overall. For reference, the first peak (peak 1) in the incident pressure graph appeared when the pressure wave front first arrived at

Table 2 Peak reflected pressure and impulse on the concrete slab

ANFO (kg)	Peak reflected pressure, P (MPa)					Impulse, I (kPa·s)				
	Exp		FEA		JWL/I&G	Exp		FEA		JWL/I&G
	P_i	\bar{P}	JWL	I&G		I_i	\bar{I}	JWL	I&G	
1	1.75	1.53	1.63	1.67	0.97	3.72	3.69	2.01	3.95	0.51
	1.39	(1.0)	(1.06)	(1.09)		3.72	(1.0)	(0.54)	(1.07)	
	1.48					2.94				
	1.47					2.97				
	1.54					3.89				
	1.49					4.17				
	1.48					4.80				
2	2.79	3.07	2.37	3.13	0.76	5.24	5.50	3.87	6.81	0.57
	2.81	(1.0)	(0.77)	(1.02)		5.24	(1.0)	(0.70)	(1.23)	
	3.74					6.15				
	3.04					5.90				
	3.93					5.87				
	2.82					4.43				
	2.76					5.24				
3	4.91	4.79	3.83	5.33	0.72	7.50	7.70	6.69	10.60	0.63
	4.10	(1.0)	(0.80)	(1.11)		7.50	(1.0)	(0.87)	(1.38)	
	4.90					8.29				
	4.40					7.99				
	5.65					7.23				
	4.46					3.67				
	4.61					9.07				

Table 3 Peak incident pressure and impulse in the shock tube (at the free 1 position)

ANFO (kg)	Peak incident pressure (MPa) peak1 (P ₁), peak2 (P ₂)					Impulse, I (kPa·s)				
	Exp		FEA		JWL/I&G	Exp		FEA		JWL/I&G
	P _{1,i} , P _{2,i}	$\overline{P_1}, \overline{P_2}$	JWL	I & G		I _i	\overline{I}	JWL	I&G	
1	0.39, 0.23	0.36	0.32	0.38	0.84,	2.69	2.42	2.05	3.04	0.67
	0.32, 0.13	(1.0),	(0.89),	(1.05),	0.78	1.92	(1.0)	(0.85)	(1.26)	
	0.34, 0.15	(1.0)	(0.74)	(0.95)		1.86				
	0.32, 0.17					2.24				
	0.39, 0.22					2.58				
	0.40, 0.22					2.68				
	0.39, 0.24					2.75				
2	0.62, 0.42	0.62	0.45	0.72	0.63,	3.95	3.74	2.55	4.59	0.56
	0.63, 0.37	(1.0),	(0.73),	(1.16),	0.57	3.91	(1.0)	(0.68)	(1.23)	
	0.84, 0.41	(1.0)	(0.63)	(1.10)		3.92				
	0.62, 0.36					4.10				
	0.62, 0.41					3.67				
	0.65, 0.44					2.85				
	0.62, 0.46					3.05				
3	0.89, 0.52	0.86	0.62	1.35	0.46,	4.07	4.03	2.83	5.95	0.48
	0.73, 0.31	(1.0),	(0.72),	(1.57),	0.45	3.51	(1.0)	(0.70)	(1.48)	
	0.97, 0.50	(1.0)	(0.61)	(1.35)		4.41				
	0.90, 0.55					4.33				
	0.82, 0.44					3.81				
	0.91, 0.46					3.27				
	0.89, 0.51					4.30				

the location, and the second peak (peak 2) occurred when the pressure wave reflected by the slab returned.

It is necessary to reduce the mesh size, calibrate the constants used in the analysis, and consider the nonlinear behavior of the structure, including crack and failure behaviors, to produce a pressure–time curve that is closer to the test results. However, as indicated by the comparison of the incident and reflected pressures, overall aspects, such as peak pressures and change in the values on the curves over time, were similar to the test results even when the explosive charge mass applied in the simulation changed. In particular, the pressure–time curve obtained using the JWL model was lower than that obtained using the I&G model for all the charge masses. According to these comparisons, the FE model used in this study (Fig. 2) was appropriate for the comparative analysis of the simulation results obtained using the JWL and I&G EOSs.

From the shock-tube tests and FE simulation, the reflected pressure curves similar to the shape of the curve represented by the Friedlander’s equation (Angelides et al., 2023; Farrimond et al., 2022) was obtained as shown in Fig. 5. Friedlander’s equation is an empirical equation used to calculate the overpressure applied

to a structure by a free-field explosion. There was a gap between the concrete slab specimen and the outlet of the shock tube, which made it possible to obtain a pressure curve that can be obtained in a free-field explosion rather than a confined explosion. It is very meaningful to present the reflected pressure–time relationship for the concrete slab in the form of Friedlander’s equation. This is because the purpose of using shock-tube equipment is to simulate a free-field environment (Stewart, 2018). For a representative example, the comparison of the reflected pressure for 3 kg of ANFO is as follows. The experimental and Friedlander curve are compared as shown in Fig. 6a. The Friedlander curve was plotted using Eq. (5), where peak reflected pressure $P_{r,max}$ was determined using the experimental mean value, and positive duration t_d was 10 ms. Decay coefficient b is 4.3, which was determined under the condition that the area of the interval corresponding to the positive duration of the curve is equal to each other.

$$P_r(t) = P_{r,max} \left(1 - \frac{t}{t_d} \right) e^{-bt/t_d} \tag{5}$$

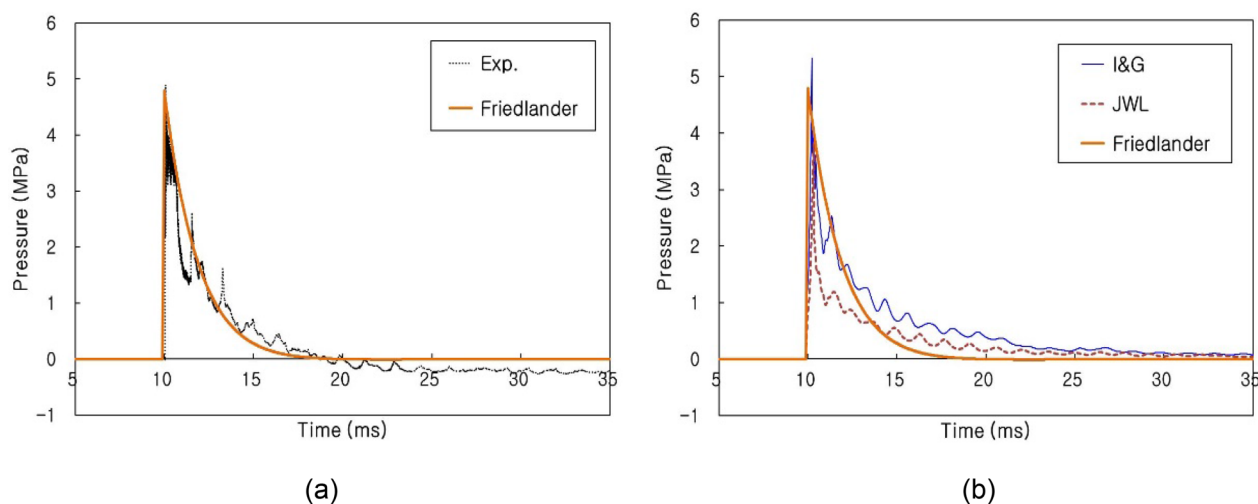


Fig. 6 Comparison of reflected pressure–time curve based on the empirical equation: **a** with curve from the experimental result and **b** with curves from the numerical analysis results

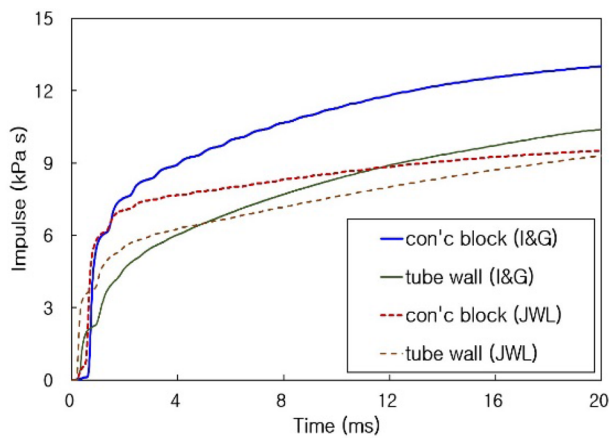
The Friedlander curve shown in Fig. 6 a can be obtained using the widely known CONWEP (conventional weapons effects) program (Hyde, 1988) or LOAD_BLAST_ENHANCED keyword in LS-DYNA. For example, under surface burst conditions, when 2339 kg of ANFO (= TNT 1778 kg, equivalent factor 0.76 (Dewey, 2020)) explodes at a distance of 15 m, the reflected pressure–time history generated on the concrete slab specimen is the same as the Friedlander curve in Fig. 6a. According to this, power generated by the explosion of 3 kg of ANFO in the shock tube is the same as that of the explosion of 2339 kg of ANFO under free-field conditions. Furthermore, the reflected pressure–time history from FE analysis and Friedlander curve are compared as shown in Fig. 6b. It can be seen that most of the initial section in the curve obtained using JWL EOS is lower than the results obtained using the Friedlander equation and I&G EOS. Since the area of the curve represents impulse, it was found that impulse may be underestimated if JWL EOS is used. More detailed analysis results related to impulse are described in Sect. 4.3 of this study.

4.3 Analysis of Influencing Factors

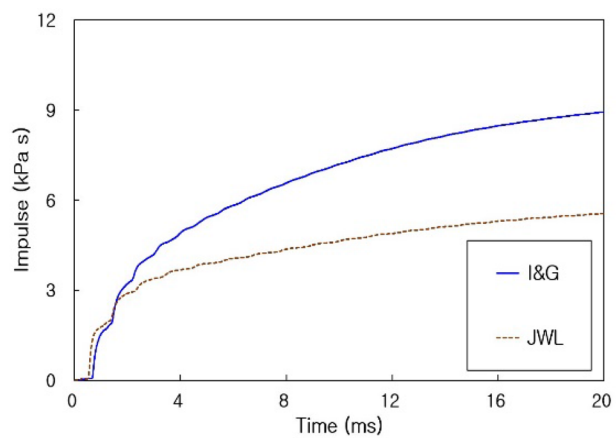
As indicated by the comparison of the pressure–time curves, differences in the simulated blast behavior could be caused by the EOS used. Here, the differences are examined in more detail. The impulses on the shock-tube wall located laterally to the explosive, at the center of the block obstructing the shock-tube inlet, at the center of the shock tube at a distance of 30 cm above the explosive, and at the center of the slab at the shock-tube outlet were compared. The impulse was determined by integrating the pressure–time curve.

Fig. 7a presents a comparison of the impulses on the shock-tube wall at the side of the explosive and the block below the explosive. These two locations were where the pressure wave generated by the detonation entered and the first reflected wave was generated. As reviewed in Sect. 4.1, the magnitude, distribution, and propagation of the blast pressure depended on the EOS used. Here, differences in blast behaviors depending on the EOS are examined in terms of the impulse. Fig. 7a presents a comparison of the impulses on the shock-tube wall. As shown, the impulse was initially larger when the JWL EOS was used, but over time, it became larger when the I&G EOS was used. However, the difference between the two results was smaller than the difference in the impulse on the block. The impulse on the block initially did not exhibit differences, but it eventually increased significantly when the I&G EOS was used. Fig. 7b compares the impulses at the center of the shock tube in the upward direction of the explosive. This was the location where the pressure wave reflected by the shock-tube wall and block passed through a series of development steps, although there were time differences. Fig. 7c presents a comparison of the impulses at the center of the slab. Fig. 7a–c shows that the blast behavior around the explosive at the beginning of the detonation continued to influence the subsequent waves until they interfered and overlapped and finally reached the slab. Moreover, as shown in Fig. 7d, the early detonation behavior leading to an increase in the impulse at the slab was identical among all the explosive charge masses.

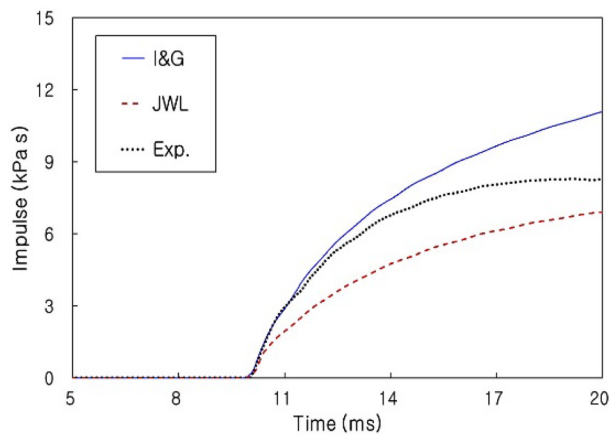
The aforementioned blast behavior is caused by various factors, such as the development process of the pressure wave in the condition of confined explosion and the



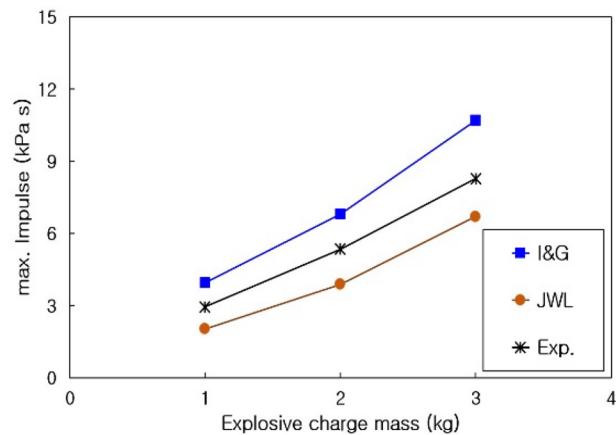
(a) At the structure surface around the explosive



(b) Near the top of the explosive



(c) At the slab surface



(d) Maximum impulse for each charge mass

Fig. 7 Impulse calculated using each EOS

release rate of initial explosive internal energy. First, the development of the pressure wave are examined. The pressure wave reflected by a shock-tube wall overlapped with other waves (reflected from the wall at different positions) at the center of the shock tube and propagated directly toward the outlet. However, at the block position, the incident pressure coming directly from the explosive and the pressure reflected by the wall interfere and overlap. The resultant pressure wave is reflected by the wall again and finally propagates toward the outlet of the shock tube. In the case of pressure development due to blocks, the pressure lasts longer. Thus, the impulse, which is defined as the product of pressure and time, is larger than that in the case of pressure development due to shock-tube walls. Second, the energy release

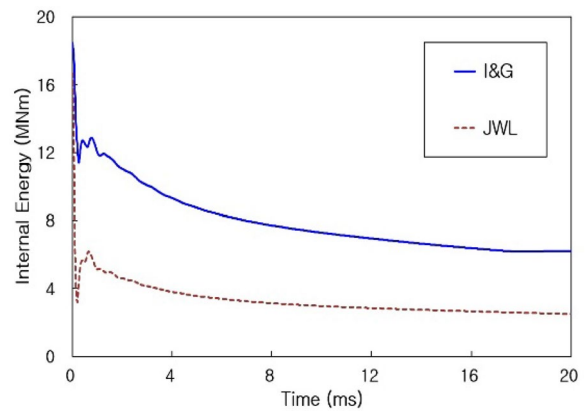


Fig. 8 Internal energy of the explosive

characteristics of explosives are examined. The JWL EOS is based on an explosion model that assumes an instantaneous detonation without considering the reaction rate of the explosive. In contrast, when the I&G EOS was used, immediately after ignition, the amount of energy released was relatively small, as shown in Fig. 8. Subsequently, the energy decreased with a constant slope according to the reaction rate of the explosive. Consequently, after the pressure increased, it gradually decreased, as reported by Elbasuney et al. (2020), and this led to an increase in the impulse.

As described above, the causes of the difference between the wall impulse and the block impulse can be briefly summarized as follows: (1) the impulse of the wave reflected by the block is larger than that of the wave reflected by the shock-tube wall owing to the difference in the development process of the pressure wave. (2) Next, the reason why the difference between the wall impulse and the block impulse is larger when the I&G EOS is used can be summarized as follows. As the energy release proceeds at a lower rate in the I&G case, the pressure decreases more slowly. In addition to the effect of the development of the pressure wave, the effect of this lower energy-release rate appears to be reflected in the increase in the block impulse. Thus, the difference in impulse is explained by two factors: the development process of the pressure wave in the condition of confined explosion and the release rate of explosive internal energy.

4.4 Parametric Study: Energy Release Rate and Wave Development Process in Confined Explosion

Differences in blast behavior between JWL and I&G EOS analyses may be caused by various factors. However, in this study, the main influencing factors were identified as

the release rate of initial explosive internal energy and the development process of the pressure wave in the condition of confined explosion. First, the energy release rate can be considered when the I&G EOS is used, and it is governed by the reaction rate equation. The second term in Eq. (4) is related to the development of pressure due to the explosion (Johansson, 2011). This term was analyzed by changing the rate constant G from 10 to 25 (unit: $10^{-11} \mu s^{-1} Pa^{-\gamma}$). In the second term of the reaction rate equation, the constants c and d are related to the burn surface topology, and γ is the power dependent on the pressure, which is a constant that affects the relationship between the diameter of the explosive and the detonation velocity (Kittel et al., 2016). Next, the influence of concrete blocks on the development process of the pressure wave in the condition of confined explosion was examined. The cases with and without blocks were analyzed, and the impulses on the slab were compared.

As shown in Fig. 9a, with the exception of the case of $G=10$, the impulse generally decreased as the G value increased, and it approached the analysis result obtained using the JWL EOS. The energy evolution of the explosives at G values of 20 and 25 in Fig. 9b indicates that the energy decreased significantly at once, similar to the JWL case. Once the shockwave reaches an obstacle, the pressure increases instantaneously and then gradually decreases. If the energy decreases faster (more energy is consumed at once), the peak pressure can increase by a larger amount. However, the decrease rate of the pressure after the peak becomes very high. Thus, the impulse, which is defined as the product of pressure and time, was calculated to be relatively small. Meanwhile, when the G value was 10, the calculated impulse was the smallest from the beginning. The peak pressure was half of the

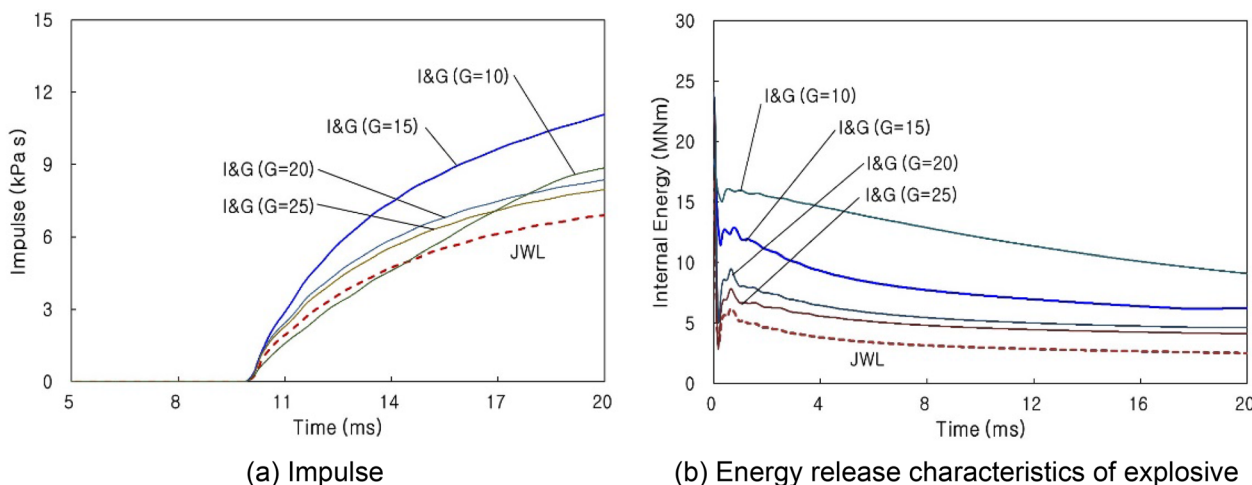


Fig. 9 Comparison of the blast behaviors with different rate constants (G). **a** Impulse. **b** Energy release characteristics of explosive

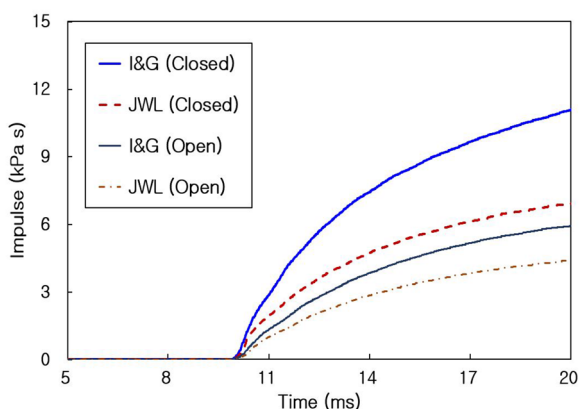


Fig. 10 Effects of concrete blocks on the slab impulse

peak pressure in the case of $G=15$, and the overall pressure level was also lower, resulting in a small impulse. Although the energy reduction was small, the calculated impulse was small because the overall pressure level was low. Thus, $G=10$ was an exceptional case.

Next, as shown in Fig. 10, the case where the inlet of the shock tube was obstructed by a concrete block (“Closed”) and the case where it was unobstructed (“Open”) were compared. Because the pressure curves obtained using $G=15$ were closest to the experimental results, the G value of 15 was used for both the main analysis and the parameter study shown in Fig. 10, where $G=15$ was a representative value as well as a fixed constant. To date, the constant G is determined via comparison with experimental and analytical results. As mentioned in the discussion section, further study is needed to determine a proper G value for general applications.

In the Open case, the impulse was significantly reduced because the effect of the pressure wave reflected by the concrete block was not reflected in the impulse. Furthermore, the difference between the analysis results for the I&G and JWL EOSs was larger when the inlet was closed. Thus, the development process of the pressure wave due to the concrete block was one of the main factors influencing the impulse, and the effect was larger when the I&G model was used.

5 Discussion

According to Furtney et al.’s study (2012) of the rock blasting process, “ANFO explosives are characterized by a relatively slow release of energy, and they also exhibit higher equilibrium pressures compared to the cases of more rapid energy release such as emulsion explosives.” This is one of several studies that explain how the energy release characteristics of explosives affect the blast behavior (Cunningham et al., 2006; Kittel et al., 2016;

Scott et al., 2023; Stimac et al., 2021). Since the JWL EOS does not take into account the energy release rate of explosives with non-ideal explosion characteristics, EOS based on reactive flow model, such as I&G EOS, should be applied to FE simulations.

Furthermore, it was confirmed that the influence of the rate constant G is crucial for analyzing non-ideal blast behaviors. Currently, there are few studies on ANFO explosives, and the value of the constant G is determined via comparison with experimental and analytical results (Jayasinghe et al., 2017; Johansson, 2011; Stimac et al., 2021). Many experimental studies are needed, because diverse parameters may be involved, depending on the composition and initial conditions of the ANFO.

6 Conclusion

The behavior of the pressure wave generated in a shock tube by the explosion of an ammonium nitrate fuel oil (ANFO), which exhibits non-ideal explosion characteristics, was numerically analyzed through an FE analysis using the Arbitrary Lagrangian–Eulerian (ALE) numerical simulation technique of LS-DYNA. The following results were obtained:

1. The behavior of the pressure wave in the shock tube was affected by two main factors: the release rate of initial explosive internal energy and the development process of the pressure wave in the condition of confined explosion.
2. Explosives with a relatively low energy release rate, such as ANFO, are characterized by a gradual reduction in explosive pressure (low decrease rate of the pressure after peak). To properly simulate the blast behavior (for example, propagation of pressure wave, pressure–time and impulse curve, etc.) in a shock tube when explosives with non-ideal explosion characteristics are used, a model that considers the reaction rates of explosives, such as the I&G EOS based on a reactive flow model, was suggested to be applied.
3. The analysis results related to the development process of the pressure wave in the condition of confined explosion were as follows. A concrete block installed at the inlet of the shock tube acted as a confinement condition that amplified the pressure generated by the explosion. The impulse produced during the generation and development of the reflected waves due to the block exceeded that produced by the shock-tube wall. This behavior was more pronounced when the I&G EOS was used, which was attributed to the increase in impulse due to the low energy release rate.

For explosives with non-ideal explosion characteristics such as ANFO, the material properties of the explosive container affect the blast behavior (Kittel et al., 2016). According to the results of the parametric analysis, the structures close to the explosives, such as the shock-tube wall and concrete blocks, also affected the blast behavior. Various boundary conditions may exist according to the geometry of the shock tube and other surrounding structures. Therefore, many experimental and comparative studies need to be conducted in further studies.

Acknowledgements

Not applicable

Author contributions

1) H.S.S.: conceptualization, methodology, simulation, validation, investigation, writing—original draft, writing—review and editing; 2) S.W.K.: conceptualization, writing—review and editing; 3) J.H.M.: methodology, validation, writing—review and editing, project management; 4) G.K.P.: investigation, experimental data curating, writing—review and editing. All authors read and approved the manuscript.

Funding

This study was supported by the KICT (Korea Institute of Civil Engineering and Building Technology) Research Program (20240176-001) Development of Technology to Secure Safety and Acceptability for Infrastructure in Hydrogen City (3/3) funded by the Ministry of Science and ICT in Republic of Korea.

Availability of data and materials

Not applicable (the data sets used and analyzed in this study are presented in the tables and the graphs of this manuscript. Other experimental data are available from the authors upon a reasonable request by the official letter).

Declarations

Competing interests

The authors declare that they have no competing interests.

Received: 10 August 2023 Accepted: 20 January 2024

Published online: 28 May 2024

References

- Angelides, S. C., Morison, C., Burgan, B. A., Kyprianou, C., Rigby, S. E., & Tyas, A. (2023). A methodology for predicting far-field blast loading on structures. *Structures*, *58*, 105619.
- Atoui, O., Kechagiadakis, G., Moumen, A., Maazoun, A., Belkassam, B., Pyl, L., & Lecompte, D. (2022). An explosive driven shock tube-based laboratory scale test for combined blast and fragment impact loading. *Applied Science*, *12*, 6854.
- Balan, G. S., & Raj, S. A. (2023). A review on shock tubes with multitudinous applications. *International Journal of Impact Engineering*, *172*, 104406.
- Bohanek, V., Stimac Tumara, B., Serene, C. H. Y., & Suceska, M. (2023). Shock initiation and propagation of detonation in ANFO. *Energies*, *2023*(16), 1744.
- Bohanek, V., Suceska, M., Dobrilovic, M., & Hartlieb, P. (2022). Effect of confinement on detonation velocity and plate dent test results for ANFO explosives. *Energies*, *2022*(15), 4404.
- Carriere, M., Heffernan, P. J., Wight, R. G., & Braimah, A. (2009). Behaviour of steel reinforced polymer (SRP) strengthened RC members under blast load. *Canadian Journal of Civil Engineering*, *36*, 1356–1365.
- Changyou, L., Jingxuan, Y., & Bin, Y. (2017). Rock-breaking mechanism and experimental analysis of confined blasting of borehole surrounding rock. *International Journal of Mining Science and Technology*, *27*, 795–801.
- Cunningham, C., Braithwaite, M., & Parker, I. (2006). Vixen detonation codes: Energy input for the HSBM. *Proceedings of the 8th International Symposium on Rock Fragmentation by Blasting*, *8*, 169–174.
- Dewey, J. M. (2020). Studies of the TNT equivalence of propane, propane/oxygen, and ANFO. *Shock Waves*, *30*, 483–489.
- Dimitraki, L. S., Christaras, B. G., & Arampelos, N. D. (2021). Investigation of blasting impact on limestone of varying quality using FEA. *Geomechanics and Engineering*, *25*(2), 111–121.
- Dobrocinski, S., & Flis, L. (2015). Numerical simulations of blast loads from near-field ground explosions in air. *Studia Geotechnica Et Mechanica*, *37*(4), 11–18.
- Elbasuney, S., Zaky, M. G., Radwan, M., Maraden, A., & Abdelkhalik, S. M. (2020). Aluminium nanoparticles: the potentials of metalized explosives with combined destructive effect. *Materials Science and Engineering*, *975*, 012009.
- Esen, S. (2008). A Non-ideal detonation model for evaluating the performance of explosives in rock blasting. *Rock Mechanics and Rock Engineering*, *41*(3), 467–497.
- Esen, S., Souers, P. C., & Vitello, P. (2005). Prediction of the non-ideal detonation performance of commercial explosives using the DeNE and JWL++ codes. *International Journal for Numerical Methods in Engineering*, *64*, 1889–1914.
- Fabin, M., & Jarosz, T. (2021). Improving ANFO: effect of additives and ammonium nitrate morphology on detonation parameters. *Materials*, *2021*(14), 5745.
- Farrimond, D. G., Rigby, S. E., Clarke, S. D., & Tyas, A. (2022). Time of arrival as a diagnostic for far-field high explosive blast waves. *International Journal of Protective Structures*, *13*(2), 379–402.
- Figuli, L., Cekerevac, D., Bedon, C., & Leitner, B. (2020). Numerical analysis of the blast wave propagation due to various explosive charges. *Advances in Civil Engineering*, *2020*, 8871412.
- Friedlander, F. G. (1946). The diffraction of sound pulses, I. *Diffraction by a Semi-Infinite Plate, Proceedings of the Royal Society of London A*, *186*, 322–344.
- Furtney, J. K., Sellers, E., & Onederra, I. (2012). *Simple models for the complex process of rock blasting. Proceedings of the 10th International Symposium on Rock Fragmentation by Blasting, Fragblast 10, New Delhi, India*. Milton: Taylor & Francis Books Ltd.
- Gan, E. C. J., Remennikov, A., Ritzel, D., & Uy, B. (2020). Approximating a far-field blast environment in an advanced blast simulator for explosion resistance testing. *International Journal of Protective Structures*, *11*(4), 468–493.
- Grisaro, H. Y., Edri, I. E., & Rigby, S. E. (2021). TNT equivalency analysis of specific impulse distribution from close-in detonations. *International Journal of Protective Structures*, *12*(3), 315–330.
- Hu, Y., Wu, C., Lukaszewicz, M., Dragos, J., Ren, J., & Haskett, M. (2011). Characteristics of confined blast loading in unvented structures. *International Journal of Protective Structures*, *2*(1), 21–43.
- Hyde, D. (1988). *User's guide for microcomputer programs CONWEP and FUNPRO, applications of TM 5-855-1*. Vicksburg: US Army Engineer Waterways Experimental Station.
- Jackson, S. I. (2017). The dependence of Ammonium-Nitrate Fuel-Oil (ANFO) detonation on confinement. *Proceedings of the Combustion Institute*, *36*, 2791–2798.
- Jayasinghe, L. B., Zhou, H. Y., Goh, A. T. C., Zhao, Z. Y., & Gui, Y. L. (2017). Pile response subjected to rock blasting induced ground vibration near soil-rock interface. *Computers and Geotechnics*, *82*, 1–15.
- Johansson, L. (2011). Numerical Study of Non-Ideal Explosive Detonations. Master's Thesis, Luleå University of Technology, Luleå, Sweden.
- Karlos, V., Solomos, G., & Larcher, M. (2016). *Analysis of blast parameters in the near-field for spherical free-air explosions*. Italy: Joint Research Center Technical Report, European Commission.
- Kevin, C., Doormaal, A., Haberacker, C., Hüskens, G., Larcher, M., Saarenheimo, A., Solomos, G., Stolz, A., Thammie, L., & Valsamos, G. (2013). *Resistance of structures to explosion effects Review report of testing methods*. Italy: Institute for the Protection and Security of the Citizen, European Commission Joint Research Centre.
- Kim, K. M., Kang, J. E., & Park, K. J. (2022). Blast pressure similarity experiments and analysis using explosive driven shock tube. *Transactions of Korean Society of Mechanical Engineers A*, *46*(1), 41–47.

- Kingery, C., & Bulmash, G. (1984). *Air blast parameters from TNT spherical air burst and hemispherical burst*. Maryland: US Army Armament and Development Center, Ballistic Research Laboratory, Aberdeen Proving Ground.
- Kittel, D. E., Cummock, N. R., & Son, S. F. (2016). Reactive flow modeling of small scale detonation failure experiments for a baseline non-ideal explosive. *Journal of Applied Physics*, 120, 064901.
- Korea Institute of Civil Engineering and Building Technology (KICT). (2022). *Measurement and evaluation of structural behavior under the blast pressure for the design of hydrogen gas storage*. Goyang-Si: Experimental Research Report; KICT & A-Best.
- Lee, E. L., Horning, H. C., & Kury, J. W. (1968). *Adiabatic expansion of high explosives detonation products; Report No. TID 4500-UCRL 50422*. Livermore: Lawrence Livermore National Laboratory.
- Lim, K. M., Shin, H. O., Kim, D. J., Yoon, Y. S., & Lee, J. H. (2016). Numerical assessment of reinforcing details in beam-column joints on blast resistance. *International Journal of Concrete Structures and Materials (IJCSM)*, 10(3), 87–96.
- Livermore Software Technology Corporation (LSTC). (2020). *LS-DYNA: user's manuals*. Livermore: LSTC.
- Mahmood, Y., Guo, B., Chen, P., Zhou, Q., & Bhatti, A. (2020). A Numerical study of an interlayer effect on explosively welded joints. *International Journal of Multiphysics*, 14(1), 69–80.
- Miao, S., Konicek, P., Pan, P. Z., & Mitri, H. (2022). Numerical modelling of distress blasting – A state-of-the-art review. *Journal of Sustainable Mining*, 21(4), 278–297.
- Park, G. K., Moon, J. H., Shin, H. S., & Kim, S. W. (2023). Blast resistance capacities of structural panels subjected to shock-tube testing with ANFO explosive. *Materials*, 16(15), 5274.
- Park, S. W., Beak, J. W., Kim, K. J., & Park, Y. J. (2021). Study on reduction effect of vibration propagation due to internal explosion using composite materials. *International Journal of Concrete Structures and Materials (IJCSM)*, 15, 30.
- Rebelo, H. B. & Cismasiu, C. (2017). A Comparison between Three Air Blast Simulation Techniques in LS-DYNA. *Proceedings of 11th European LS-DYNA Conference 2017*, Salzburg, Austria.
- Rigby, S. E., Knighton, R., Clarke, S. D., & Tyas, A. (2020). Reflected near-field blast pressure measurements using high speed video. *Experimental Mechanics*, 60, 875–888.
- Rigby, S. E., & Sielicki, P. W. (2014). An investigation of TNT equivalence of hemispherical PE4 charges. *Engineering Transactions*, 62(4), 423–435.
- Salvado, F. C., Tavares, A. J., Teixeira-Dias, F., & Cardoso, J. B. (2017). Confined explosion: The effect of compartment geometry. *Journal of Loss Prevention in the Process Industries*, 48, 126–144.
- Sanchidrian, J. A., Castedo, R., Lopez, L. M., Segarra, P., & Santos, A. P. (2015). Determination of the JWL constants for ANFO and emulsion explosives from cylinder test data. *Central European Journal of Energetic Materials*, 12(2), 177–194.
- Scott, D. G., Cummock, N. R., & Son, S. F. (2023). Small-scale characterization of shock sensitivity for non-ideal explosives based on imaging of detonation failure behavior. *Propellants, Explosives, Pyrotechnics*, 48, 202200252.
- Stewart, J. B. (2018). *Influence of Test Section Geometry on the Blast Environment in an Explosively Driven Conical Shock Tube Technical Report, ARL-TR-8335*. Maryland: US Army Research Laboratory.
- Stimac, B., Skrlac, V., Dobrilovic, M., & Suceska, M. (2021). Numerical modelling of non-ideal detonation in ANFO explosives applying Wood-Kirkwood theory coupled with EXPLO5 thermochemical code. *Defence Technology*, 17, 1740–1752.
- Stolz, A., Millon, O., & Klomfass, A. (2016). Analysis of the resistance of structural components to explosive loading by shock-tube tests and SDOF models. *Chemical Engineering Transactions*, 48, 151–156.
- Trofimov, V., & Shipovskii, I. (2020). Simulation fragmentation of samples of rock at explosive loading. *Proceedings of International Scientific Conference—problems of complex development of georesources. E3S Web of Conference*, 192, 01013.
- U.S. Army Corps of Engineers(USACE), Naval Facilities Engineering Command(NAVFAC), & Air Force Civil Engineer Support Agency(AFCESA) (2008). *Structures to Resist the Effects of Accidental Explosions; Unified Facilities Criteria (UFC); UFC 3-340-02*, USA.
- Yang, D., Zhang, B., & Liu, G. (2021). Experimental study on spall resistance of steel-fiber reinforced concrete slab subjected to explosion. *International Journal of Concrete Structures and Materials*, 15, 23.
- Yi, C., Nyberg, U., Johansson, D., & Schunnesson, H. (2020). Ignition and growth reactive flow model for aluminized emulsion explosive. *Proceedings of the 46th Annual Conference on Explosives and Blasting Technique, Denver, Colorado, USA*.
- Zakrisson, B., Wikman, B., & Haggblad, H. A. (2011). Numerical simulations of blast loads and structural deformation from near-field explosions in air. *International Journal of Impact Engineering*, 38(7), 597–612.

Publisher's Note

Springer Nature remains neutral with regard to jurisdictional claims in published maps and institutional affiliations.

Hyun-Seop Shin is a Research Fellow of Korea Institute of Civil Engineering and Building Technology (KICT). His recent research interest focuses on the blast-resistant structures and finite element analysis thereof.

Sung-Wook Kim is a Senior Research Fellow of KICT. His research interests include the development of ultra-high performance concrete materials and structures, and the blast-resistant materials and structural applications.

Jae-Heum Moon is a Research Fellow of KICT. His research interests focus on the nano-concrete and its applications, the blast-resistant design for hydrogen storage facilities, and the blast-resistant concrete materials.

Gang-Kyu Park is a Researcher of KICT. His recent research interest includes the blast-resistant design for hydrogen storage facilities, and finite element analysis using CESE (Conservation Element / Solution Element) method.